A Study of Segmentation and Glaucoma Diagnosis through Fundus Images using Deep Convolution Neural Network with Transfer Learning Techniques

K.Subha[1], Dr.S.Kother Mohideen[2]

[1]Reg.No 18221252162003, Research Scholar, Department of IT, Sri Ram Nallamani Yadava College of Arts & Science (Affiliation of Manonmaniam Sundaranar University) Tenkasi, Tamilnadu – 627804, India.

[2]Associate Professor & Head, Department of Information Technology, Sri Ram Nallamani Yadava College of Arts & Science Tenkasi, Tamilnadu – 627804, India.

Abstract

Retinal dysfunction glaucoma is the leading cause of vision loss in the elderly people over 40 due to high intraocular pressure (IOP). If ignored, glaucoma can damage the eye's optic nerve, leading to permanent vision loss. Glaucoma also worsens with time. The optic nerve, which transmits images from the eye to the brain, can be damaged if pressure builds up inside the eye. Glaucoma can cause irreversible vision loss if it does not receive treatment for damage to the optic nerve caused by high eye pressure. Blindness and visual impairment can be avoided with early detection and treatment. Automated retinal analysis technologies assist patients save time, money, and their vision when compared to traditional manual diagnosis procedures. Finding the Optic Disc (OD) in retinal images is essential for accurate diagnosis in this situation. Here, the optic disc and optical cup (OC) are fractured using a Improved Deep Convolution Neural Network with transfer learning . The CDR value is then calculated using a deep learning method based on the CDR structure. Images with and without glaucoma can be differentiated using different degrees of information extracted from the original image. In this proposed methods using wavelet based denoising for pre-processing the fundus images . In this proposed method using best approaches and two comparable neural network using deep convolutions architectures the optic disc and optic cup should be removed, one method produces faultless results. SCES,ACRIMA datasets were used to test and train the OC and OD segmentation design. The success rate in diagnosing glaucoma was found to be 96 percent using this data set.

Keywords: Glaucoma, Optic Cup, Optic Disc, CDR, Convolutional Neural Network, Deep Convoloution Neural Network, Transfer Learning

1. INTRODUCTION

Glaucoma affects the visual nerve and is persistent and incurable that has been linked to a wide range of visual impairment [1]. Glaucoma affects around 65 million individuals worldwide, according to the WHO [2]. Early detection and treatment are critical to avert visual loss because of the disease's asymptomatic nature. In order to keep tabs on the progression of glaucoma, doctors frequently used the retinal fundus depicted in figure 1. Inflammation of the optic nerve and/or increased intraocular pressure are the primary symptoms of this silent eye disease. It has been established that measuring IOP does not serve as a good glaucoma indicator since visual impairment might occur without an increase in IOP.
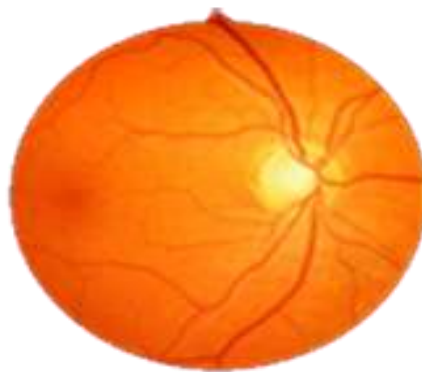

Figure 1. Fundus image of an eye

Inflammation of the optic nerve and/or increased intraocular pressure are the primary symptoms of this silent eye disease. It has been established that measuring IOP does not serve as a good glaucoma indicator since visual impairment might occur without an increase in IOP.

$$CDR = areaCup / areaDisc \qquad\qquad (1)$$

If the CDR is less than or equal to 0.6, the patient has glaucoma; otherwise, they do not. As a result of this and the literature analysis, the first stage in doing automatic glaucoma diagnosis is to get disc and cup segmentation as illustrated in Figure 2.

Glaucomatous eyes have a bigger cup compared to their normal counterparts because the optic disc (OD) is much smaller in size. In order to help with the diagnosis of glaucoma using colour fundus photographs, various approaches for segmenting the optic cup and disc have been devised. Others [4, 5] calculate the Cup/Disc ratio whereas others [4, 5] focus solely on optic cup and/or disc segmentation. (CDR). Glaucoma indicators frequently employ this parameter to express the optical disc-to-cup diameter ratio. CDR measurement, on the other hand, necessitates considerable work in order to get an precise optical disc and optic cup segmentation.

Automated search techniques typically include five components. There is a lot of pre-processing that goes on before any of these other steps. To begin, a Gaussian filter and image normalization will be applied to the input image as part of the pre-processing process. Noise and uneven illumination are reduced using a Gaussian filter in this case. Each fundus image's colour and local illumination are then balanced via image normalization. Image quality will be improved, as well as background noise will be reduced, with this technique. To analyze fundus images and recognize retinal structure, such as hemoptysis diagnosis, contoured disorders, and circulatory retrieval, the color-texture descriptor technique can be utilized. We'll look at things like arteries and retinal veins to further segment the blood vessels. By increasing the number of layers in the Enhanced deep learning DCNN model, we can extract more features during segmentation. Our optic disc and cup segmentation algorithms have been enhanced over previous studies by using an up- and down-sampling strategy on the DCNN layers. Up sampling and down sampling both keep the image resolution largely the same. As a result, throughout the training phase, more parameters can be gleaned from the data. Because of this, it assists in locating the OC and OD with more accuracy. If an image appears to show a glaucomatous eye, If the eye is healthy, the detection cup-to-disc ratio can be utilized to identify it.
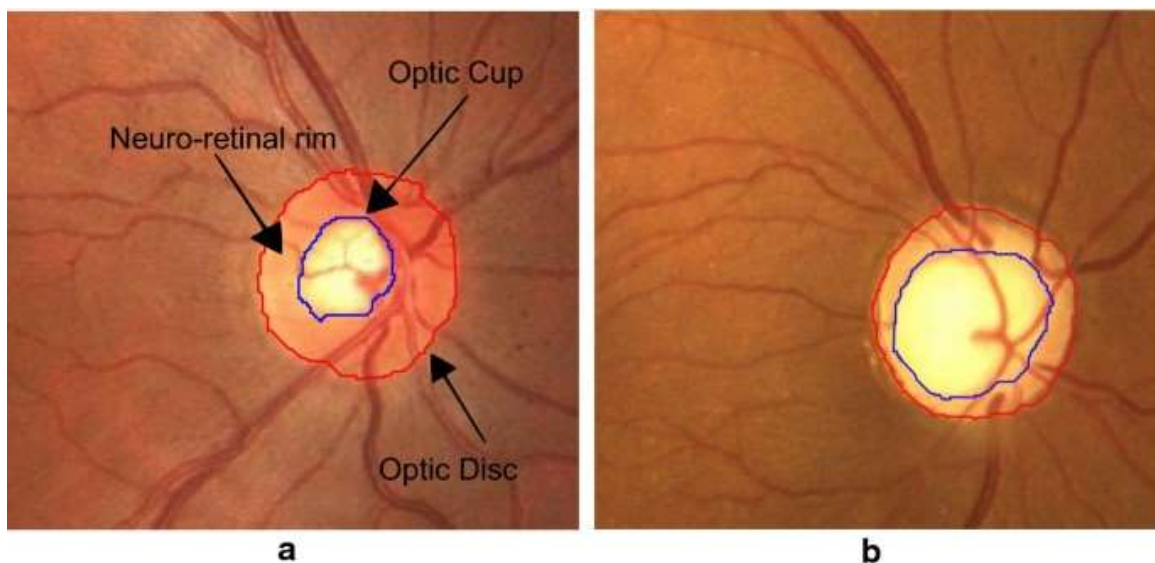

Figure 2. Cropped digital fundus images around the optic disc . (a) The main components of a healthy optic disc and (b) glaucomatous optic disc

2. LITERATURE SURVEY

During treatment, it was critical for patients to have a correct diagnosis of glaucoma. Doctors have looked at a number of diagnostic criteria, and the ones they've found focus on the area on or surrounding the optical disc. Size, location and centering of the optical disc are all precisely measured, it can help with automatic image interpretation. Many investigations have been proposed in the literature to identify the optic disc (OD). A lot of these research are concerned with two things: locating the optic disc, which means pinpointing its location in a Segmenting the optic disc region refers to finding the exact location of the optic disc. It's possible to divide the approaches used to detect optical discs into three categories: those that use morphology, templates, and model-based deformability. In 2016 the OD's origin centre might be located using vessel inpainting, as suggested by [7]. Find the OD centre first, then make use of the points you've earned by implementing adaptive region growth based on threshold . After accurate inpainting of blood vessels for removing intensity modulation of the optic disc's vascular structure was proposed by [8], followed by region growth with the optic disc centre as a seed point for reliable fundus picture segmentation. These three steps were used to detect the OD boundary. In 2017, [9] used a strategy based on Mathematical morphology to segment the OD using a canny edge detection technique backed up by other morphological processes. [10] A method for disc navigation and cup fragmentation utilizing autonomous template matching and threshold method was explored in 2017 by Septiarini et al. for glaucoma assessment. . Using masking and edge detection, this approach prevents areas from being incorrectly classified. OD segmentation algorithm reported by [11] use an image of a localised O.D. to create a segmentation level set for O.D. An inpainting method was utilised to prevent interfering with the level-setting process. For learning the picture features, Chen et al. (2015)

suggested an improved CNN-based method. When compared to the standard method, which uses a modified CNN, this method uses micro neural networks to increase the system's structure, resulting in increased network complexity. Pictures with and without glaucoma can be distinguished using this technique, the photos have been organised hierarchically. To enhance visibility of both the OD and OC in the input image, researchers developed a strategy presented by Chen et al. (b) in 2016. This approach concentrated more on morphological operations done to the image. The OD and boundary extraction are located using algorithms like the grow cut approach and the Circular Haugh transform. Bharkad and co-authors published a study in 2017 on a method for blurring blood arteries while simultaneously increasing visual contrast (Bharkad, 2017). Zahoor and Fraz (xxxx) proposed and Zahoor et al. developed an OD locating strategy utilising The Polar Optimization Technique and the Circle Hough Transformation are both used for fragmentation.

Ayub et al. [12] suggest segmenting cups and discs using RGB and HSV colour models, as well as K-mean clustering. A 92% accuracy rate has been achieved, although a disc's vascular system interferes with the accuracy of identifying correct disc pixels. Nikam and Patil [13] perform disc and cup segmentation by minimising a distance cost function using an elliptical fitting technique. . In addition, they offer a MATLAB-based user interface. Using a 32x32 minimum filter, [14] estimated the ROI to be 135x135 pixels. To identify the picture's edges, he employed the Canny Side analyzer. To keep the OD area contained, he exclusively employed the RGB green technique. The identical strategy was examined by [15]. he began by dividing the image into nine nine-pixel squares, and then selected as the disc's centre point the brick with the greatest number of pixels in the disc's brightest five percent. [3] made use of a window and a proper thersholding. As far as size went, it was a good match for the ship. He also discovered a link between the retina's green channel and the colours blue and red. As a result, a channel red was selected due to its poor blood vessel density, which could throw off the localization algorithm's basic assumptions. Based on the photo histogram, a threshold for optimal performance was chosen. After starting with a high value 11, the intensity was gradually reduced until it reached a low valueI2to generate at least a thousand identically-intensified pixels. It was successful in a subset of the histogram. The two intensities' mean values,11 and 12, were used to determine an optimum threshold. Fuente-Arriaga et al. looked for glaucoma by measuring the displacement of blood vessels within the disc. As a starting point, remove vascular tissue from the optic disc and insert it into the cup's ISNT. The nostril, inadequate, and superior filaments are taken into account for determining L1 displacement on each side of the ordinal point and the vascular groupings' centroid . It was tested on 68 images and found to have 92.56 percent accuracy in terms of retinal quality and clarity from private reports. The same approaches were employed by [12] to discover glaucoma. The ISNT and CDR quadrants were measured, and the results were used to classify a photograph as glaucomatous or not. There is a violation of the ISNT regulation when the cup-to-disc ratio goes over 0.6. Ahmad et al. processed 90 pictures with the DMED dataset.

3. MATERIALS AND METHODS

In order to evaluate glaucoma classification systems, there are only a handful publicly available datasets with glaucoma-labeled photos. As a result, the authors are happy to announce the release of ACRIMA, a new glaucoma-specific database. The ACRIMA project was initiated by Spain's Ministerio de Economa to develop automated algorithms for evaluating retinal diseases.

There are 705 images in the ACRIMA fundus image database (396 glaucomatous and 309 normal images). They were taken from glaucomatous and undamaged persons as part of the ACRIMA experiment in line with the ethical criteria set forth in the 1964 Helsinki Declaration. All of the patients were selected by experts after a comprehensive review that took into account their criterion and clinical findings. Photographs obtained with eyes already dilated and focused on the optic disc make up the vast majority of the fundus images in this collection. Some of them were removed because of the flaws in them, such as artefacts, noise, and low contrast. Capturing the images was accomplished through the use of the The IMAGE visualising collection system and the Topcon TRC retina lens are both used. Field of view was set to 35 degrees for the photography. We used two 8-year glaucoma veterans to review the ACRIMA database and comment all of the photos we could find there. While providing labels for the photos, there was no consideration of any further clinical data. The ACRIMA database's initial edition was limited to categorization tasks. Segmentation using an optical disc or an optical cup is not available. Figure 3 shows several photos culled from the ACRIMA database.
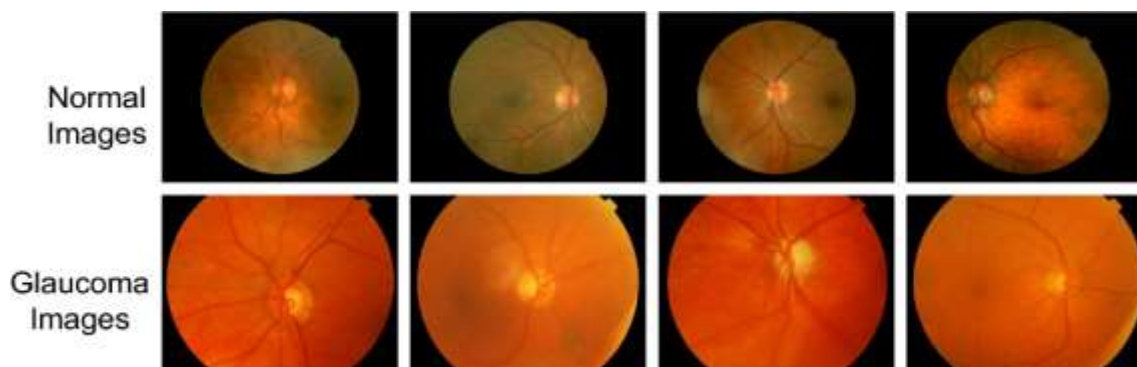

Figure 3. Normal Vs Glaucoma Images

The cup-to-disc ratio must be measured and split accurately in this assessed task in order to achieve excellent results in glaucoma identification. The whole system flow may be seen in Figure 4, which you can see below. Dimensions of the fundus photograph (2987x1987 pixels) were provided as an input parameter. The initial stage in improving the quantity and quality of a photograph was to use Waveelt based threshold methods to remove the noises . A 516x516 pixel area was clipped after the glaucoma was located at the desired location. For the division of OD and OC, two distinct 50-layer Convolutional Neural Network designs were created. Two other designs used the modified image as inspiration. From the edges of **both designs, it gives the judged mask.**
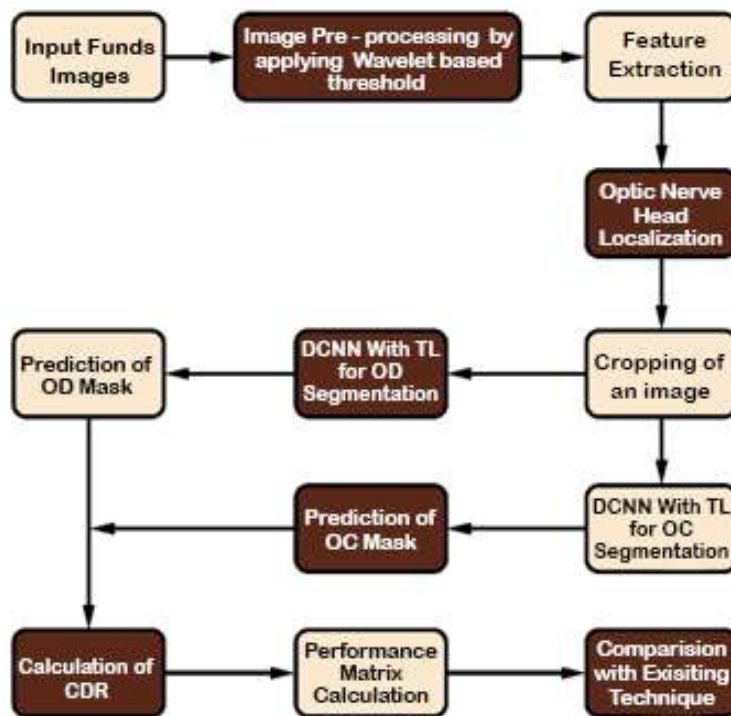

Figure . 4. System Work Flow

4. Pre-Processing

For the diagnosis of fundus photographs, this step was critical. Gaussian white noise, salt and pepper noise all have an effect on the fundus photos. A key part of the ophthalmologist's diagnosis was to get rid of any noise in the images. In fundus photographs, a filter similar to Gaussian was employed to eliminate Gaussian noise. The colours blue, green, and red are all mixed together in one channel here. This was handed off to another department.

4.1 Wavelet Based Image Denoising

Noise is present in all digital photographs to some extent. The image denoising algorithm tries to eliminate the noise in the image. The resulting denoised image should ideally be free of noise and artefacts. The capacity of wavelet approaches to capture the energy of a signal in a few energy transform values makes denoising of natural photographs affected by Gaussian noise particularly successful. The discrete wavelet transform-based image processing technology Figure 5 depicts the three phases involved in denoising.
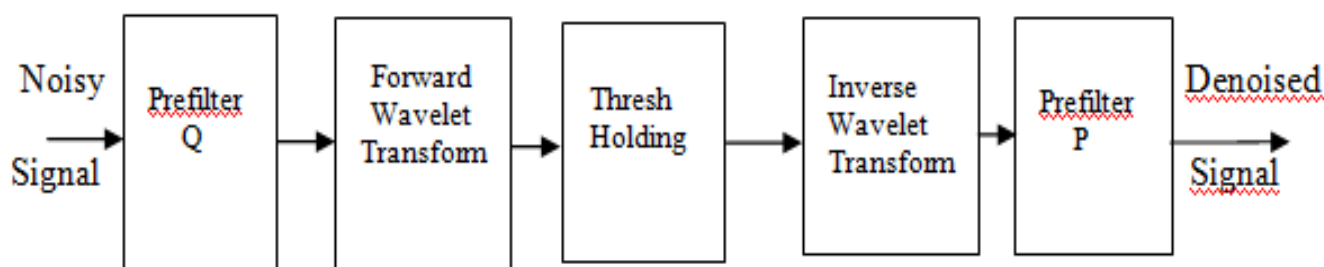

Figure 5 Wavelet Based Image Denoising

1.   Uses a discrete 2D wavelet transform to transform a noisy image into an orthogonal domain.

2.   Thresholds the wavelet transform's noisy detail coefficients, either hard or soft.

3.   To obtain the denoised image, performs the inverse discrete wavelet transform.

4.2 Types of Thresholds

Figure 6 depicts the soft and hard thresholds, which are the most commonly utilised thresholds. The noisy pixels are killed or shrunk by the soft threshold, whereas the noisy pixels are kept or killed by the hard threshold.
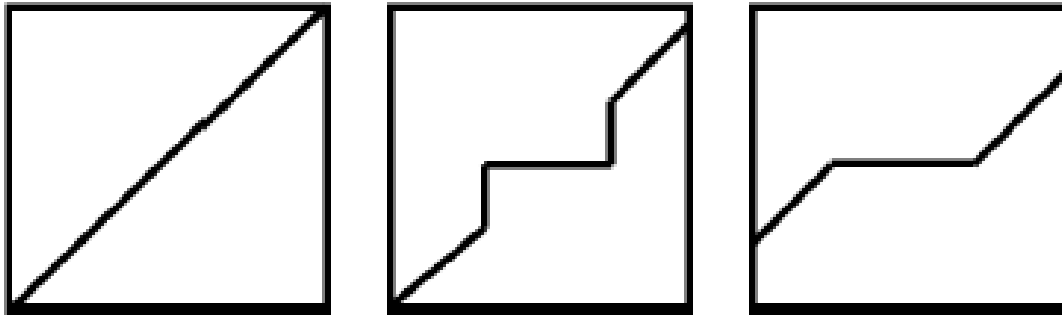

Figure 6 : (a) Original signal (b) Hard threshold (c) Soft threshold

4.3 The followings are the thresholds methods

i)VisuShrink

Donoho and I. M. Johnstone introduced VisuShrink which is calculated from diagonal sub-band HH1 as:

$$\sigma \frac{median|HH1|}{0.6745} \qquad (2)$$

Instead of minimising the mean square error, VisuShrink sets a near-optimal threshold. VisuShrink, on the other hand, has an excessive smoothing problem because it removes a significant number of high frequency coefficients, resulting in the loss of features and edge information. Another disadvantage is that it cannot reduce multiplicative noise, such as speckle noise. It only works well with additive Gaussian noise.

ii) BaysShrink

The Bays[11] shrink, which decreases Bayesian risk, employs a soft threshold that is sub-band dependant, meaning that a decomposition level threshold is applied at each sub-band. The Bayes threshold Tb is defined as:

$$TB = \frac{\sigma^2}{\sigma s} \qquad (3)$$

Where σ^2 is variance of noise which is calculated from equation (1) σs is the variance of signal. As the noise and the signal are independent of each other which is given by:

$$\sigma n^2 = \sigma s^2 + \sigma^2 \qquad (4)$$

Where σn^2 is defined as:

$$\sigma n^2 = \frac{1}{M*N} \sum_{i=1}^{M} \sum_{j=1}^{N} I(i,j)^2 \qquad (5)$$

where M*N shows the number of pixels in image I Finally, the signal variance σs^2 is calculated as:

$$\sigma s^2 = \sqrt{max(\sigma n^2, \sigma^2), 0} \qquad (6)$$

For each decomposition level, three different thresholds for diagonal, vertical, and horizontal sub-bands are calculated. Further decomposition level thresholds are calculated in the same way for each sub-band at each level.

iii) Normal Shrink

Normal Shrink TN is defined as:

$$T_N = \Lambda \frac{\sigma}{\sigma std} \qquad (7)$$

Where Λ is defined as:

$$\Lambda = \sqrt{log(Lk/L)} \qquad (8)$$

The length of the kth scale sub-band is represented by LK, while the total number of decomposition levels is represented by L in the preceding equation. is the noise variance, which has already been defined in equation (3.12). Similarly, equation can be used to find the standard deviation std of a noisy signal sub-band (3.13). Normal Shrink is used to perform a soft threshold.

iv) NeighShrink

The noisy values are reduced using NeighShrink's sliding window method. A window of LxL size is constructed, and the window's central pixel is replaced with a new value. After that, the window is shifted one pixel forward, and the same action is performed on all pixels. It's also a band-dependent shrinkage rule, with shrinking applied to each decomposition level's sub-band.If B(i,j) is the window and w(i,j) is the central pixel then the pixel w(i,j) is replaced by W(i,j) as:

$$W(i,j) = w(i,j) * B(i,j) \qquad (9)$$

Where B(i,j)is known as shrinkage factor and is defined as:

$$B(i,j) = 1 - \frac{TU^2}{s(i,j)^2} \qquad (10)$$

Image is separated into high and low frequency band and above operation window operation is conducted on all high frequency bands. As a result, each pixel value in HH, HL, and LL is replaced. Finally inverse stationary wavelet transform is used on LL, HH, HL, LH to yield demised image.

Evaluation Criteria

The above said methods are evaluated using the quality measure Peak Signal to Noise ratio which is calculated using the formulae,

$$PSNR = 10\log_{10}(255)^2/MSE \ (db) \qquad (11)$$

where MSE between the original image and the reconstructed denoised image is the mean squared error. It is used to compare various denoising schemes such as the Wiener filter, Visushrink, Neighshrink, and Modified Neighshrink. The above wavelet thresholds methods are implemented for different fundus images. The Neigh shrink method is proved outperformance results compared with the other methods. This denoised fundus images are used for further processing.

5. Improved Deep Convolution Neural Network with Transfer Learning

Deep Cropping will be performed on the image when the disc has been placed on it. . A 2788x1978-pixel Convolution Neural Networks DCNN with Deep Learning The Convolution Neural Networks are commonly used for image recognition, classification, and detection of object. DL-based CNN, known as the DCNN, has a variety of layer panels with a different set of filters. These filters are used for dimensional reduction and feature extraction. The input in the DCNN is passed in a series manner to the CL [COventional Layer] with Kernel Filters' use. This process is used for classifying the object. This model creates a probability value that ranges from zero to one for the given input value. CL layer of the DCNN is made of pooling, filters, ReLu, Dropout, and entirely connected layers. The softmax and the sigmoid function present in the DCNN are used for the classification process. The classification in DCNN is done in 2 ways. The multiclass classification is done with the help of softmax, and the binary classification is done with the help of sigmoid function. The extraction and automatic feature extraction in DCNN will always yield better results employing performance. In this paper, DCNN along with TL is employed along with the Inception V3. The Inception V3 is trained already. Figure 7 explains the TL process in detail. The Inception V3 consist of 312 layers. This process requires more datasets for the purpose of optimizing the result as well as for training. In the case of the medical sector, it is challenging to get a large amount of dataset where the smaller dataset faces the problem of overloading.
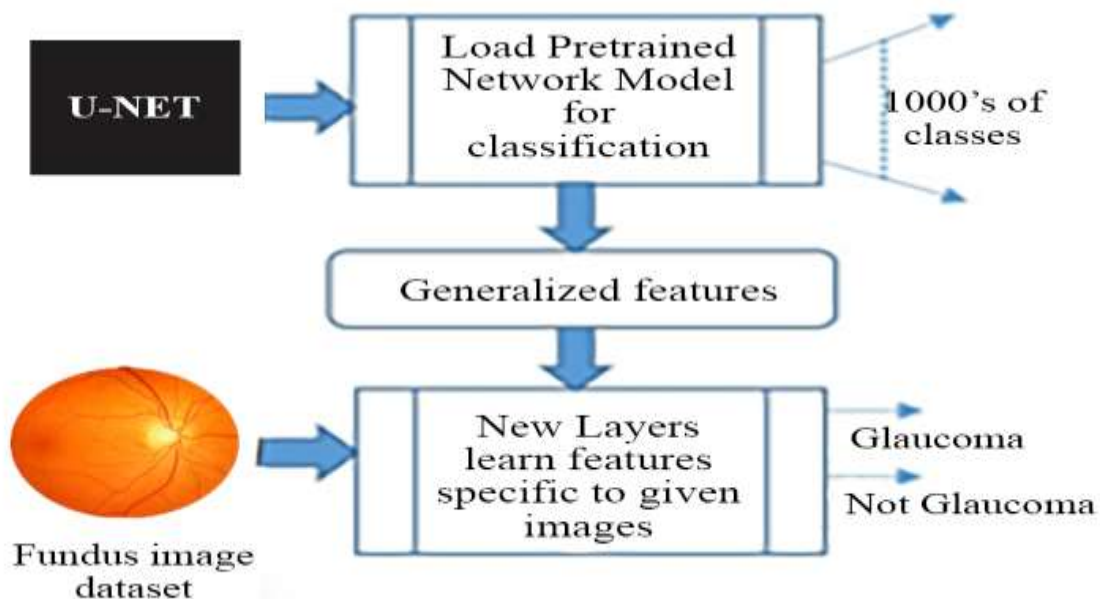

Figure 7 DCNN with TL

6. Methodology for segmenting data using a Improved DCNN with Transfer Learning

To check for glaucoma, a modified version of CNN divided the optic cup and disc into two halves. The division method was made more precise using two distinct convolution neural network designs. During the division procedure, identical layers were placed to the optical disc and the optical cup, respectively. The neural network model with convolutional layers for image training did not have as an input the size of the entire fundus picture of 2200x1400. The convolutional neural network model used a clipped image of 132x132 pixels in the nerve region as an input to reduce implementation time. With the addition of the 45th layer, there are now 42 layers in the convolutional neural network model. These levels include merge, upsampling, convolutional, and drop out. Instead of using individual RGB images to divide the channel, the complete RGB image was utilised. Convolution was used to construct a map out of the two sets of data after various filters were examined. Reducing the image size is as simple as choosing the high values from the layer's max-pooling groups. It is possible to reduce dismissal by using convolutional neural networks and down sampling analysis to focus on certain activation marks. Up sampling helps to restore the lost data. The selected data was removed using a dropout layer on every convolution operation. and prevent it from over fitting in CNN. When using ReLu activation, it helps to train the design while also providing the best possible process in relation to the other processes. 00 and 10 were shown as pixel values in the binary mask of the optical disc as a result. When a pixel's value is close to the original, it will appear as a black or white dot. Another design used the assessed optic disc mask to examine the optic cup mask. Because of this, the edge of the optical cup cannot be accurately determined with the current technique. The problem will be analysed when the optic disc mask study yields ideal results. The size of the image used to judge the optical cup in the first design, in which the optical disc picture size was taken into consideration . The original concept for the OC was scrapped in favour of the third. Cup-to-disc ratio measurement was used to determine whether or not this person had glaucoma..

7. Training and Modelling

The division procedure made use of two different modified layers of convolutional neural networks. This aids in honing the layer's symmetry. For the development of the convolutional neural network model, we used the Tensor Flow and Kera's . The first model divides OD using 50 layers, dropout, convolution, merge layer, and down and up sampling are all examples of this technique. . The first design used a cropped image 130x130 pixels as an input. Second convolutional neural network model used same-layer input (520x520) for OC prediction. The total number of parameters is 600,200, the number of parameters that can be trained is 600,200 and the number of parameters that cannot be trained is zero.

8. Prediction

Whether the cup-to-disc ratio can be improved was useful in monitoring glaucoma progression, this research set out to find out. These experiments yielded data from which the cup to disc ratio was derived. The value of CDR was determined using the square root of the disc region proportion. Pixels that are white are used to create the OC and OD fields, respectively.
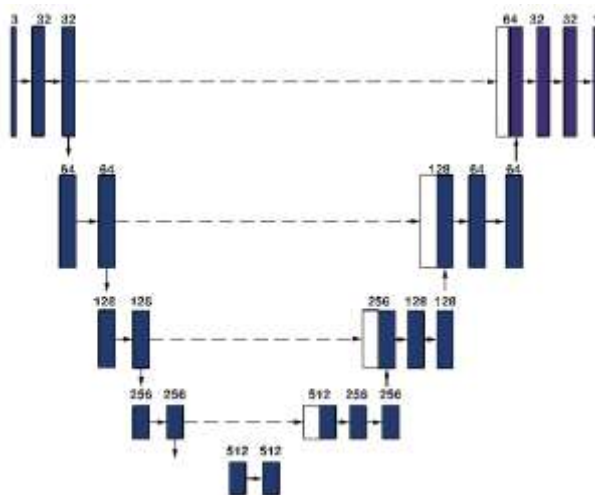

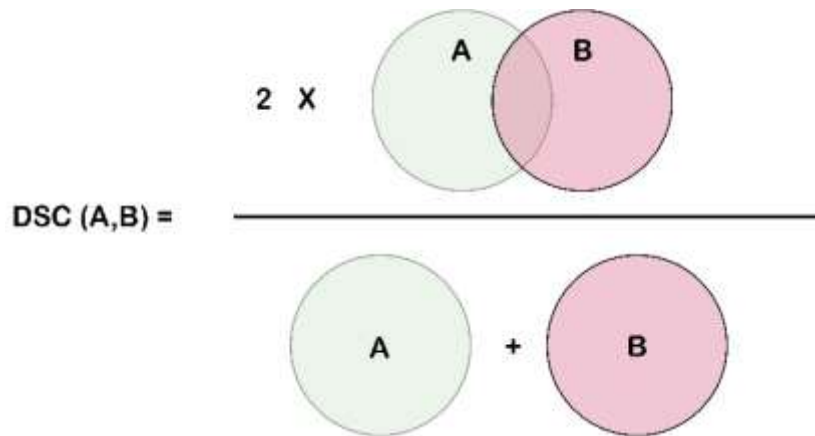Figure 8   UNET Architecture used to identify CDR

9. RESULTS AND DISCUSSION

Training the design was place on a structured equipped with good graphics card. Several metrics have been presented to analyse the outputs, and the outputs are linked to the resulting system.

9.1 Dice similarity coefficient

Set A and B's dice metrics will be calculated as

$$DSC = \frac{2|A \cap B|}{|A| + |B|}$$

The symbols |A| and |B| signify the sets A and B, respectively. Equations 1 and 2 produce the dice metric equation. Depending on the context, it can alternatively be stated as TN, FN, TP, or FP.

$$\text{Dice Coefficient} = \frac{2 \times Intersection}{Union + Intersection} = \frac{2TP}{2TP + FN + FP}$$

9.2. Intersection over union (IOU)

In the division process, IOU is frequently employed as a common metric. It's the area ratio calculated by joining the areas together, and it's displayed as a set of sets so you can see how they differ. The Jaccard Index is another name for it. The IOU is expressed as a percentage.

$$IOU(A, B) = \frac{|A \cap B|}{|A| + |B| - |A \cap B|}$$

$$IOU = \frac{\text{area of overlap}}{\text{area of union}}$$

9.3. F1 score

The output accuracy was calculated using the F1 score. It also verified the binary value's classification. In terms of recall and precision, this is the case. The following formulae can be used to calculate it.

$$\text{Precision} = \frac{\text{True Positives}}{\text{True Positives + False Positives}}$$

$$\text{Recall} = \frac{\text{True Positives}}{\text{True Positives + False Negatives}}$$

$$F_1 = 2 * \frac{\text{precision} * \text{recall}}{\text{precision} + \text{recall}}$$
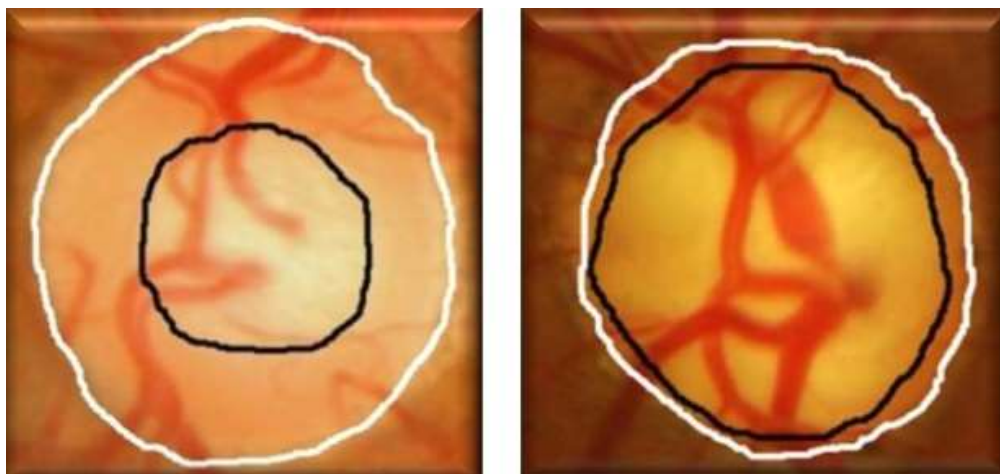
(a)   (b)

Figure .9 Fundus Image (a) and Glaucoma (b) OD region-of-interest (ROI) image demonstrating the effect of rim dilution caused by glaucoma eye illness.

9.4. Structural similarity Index (SSIM)

Images and videos were compared with Structural Similarity Index. The formula is shown in the equation below.

$$SSIM(x,y) = \frac{(2\mu_x\mu_y + c_1)(\sigma_{xy} + c_1)}{(\mu_x^2 + \mu_y^2 + c_1)(\sigma_x^2 + \sigma_y^2 + c_2)}$$

The lx variable represents the average value of x, the ly variable represents the average value of y, the r2 variable represents the variance of x, the r2y variable represents the variance of y, and the covariance of is represented by rxy.

9.5. Accuracy

Equation 6 calculates the percentage of correctly categorised pixels in the image.

$$Accuracy = \frac{TP+TN}{TP+TN+FP+FN}$$

9.6. Mathews correlation coefficient (MCC)

The quality of binary division was calculated using the Mathews correlation coefficient.

$$MCC = \frac{TP \times TP - FP \times FN}{\sqrt{TP+FP}(TP+FN)(TN+FP)(TN+FN)}$$

Measuring with an optical cup or disc requires measuring all of the relevant parameters. When a design has been tested and trained numerous times, the parameters are assessed to assess its overall performance. OC and OD precision are shown in Table 1 with various measurements. One thousand epochs of the metrics performance are used to test and train the evaluated technique. The metric dice, on the other hand, served as the foundational metre for correlating the learned techniques. The tab displayed this information. When layers are upgraded, mistakes are less likely to occur. As you can see in Figure 10, the training data for dice metrics vs loss in OD division is plotted over 1000 repetitions. Figure 11 shows the curve there have been 1000 iterations of the dice metric compared to the loss in the OC division . Finally, the OC and OD divisions achieved results of 96 percent and 96 percent for training information

Table 1 Performance metrics measurement for disc and cup segmentation. Using proposed DCNN with Transfer learning

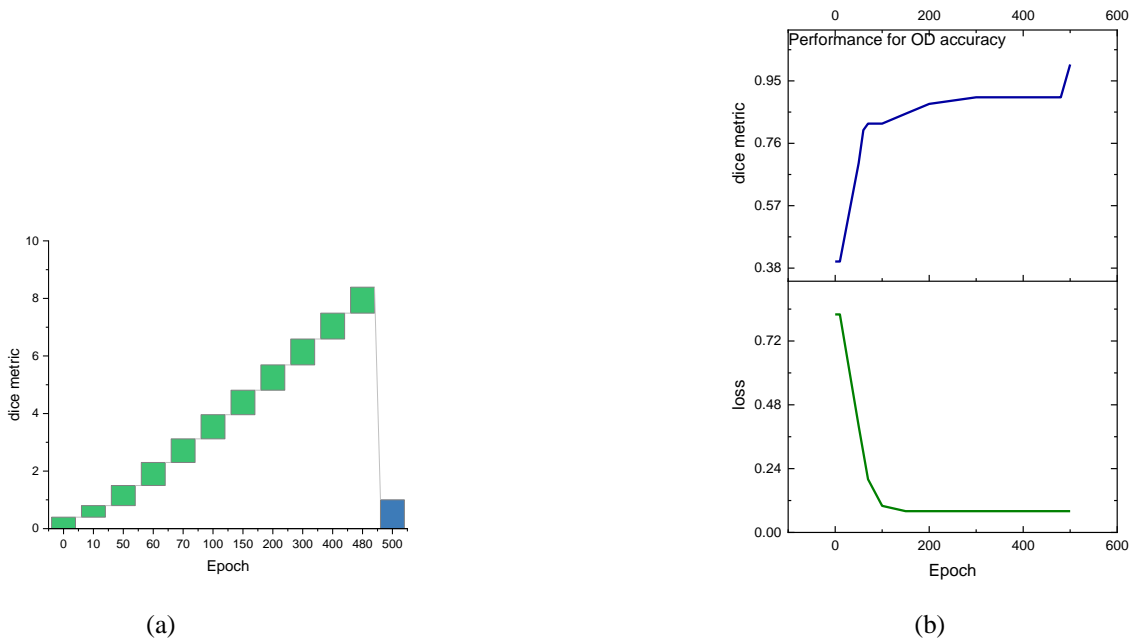| Accuracy Metrics	Disc Segmentation	Cup Segmentation
Dice Metric	0.9782	0.9811
IOU	0.9128	0.9121
F1 Score	0.9642	0.9342
SSIM	0.9389	0.9148
Accuracy	0.9616	0.9612

(a)

(b)

Figure 10 (a) Graphical representation between the dice metric of OD and the 500 epochs of trained data. (b) Comparison graph between the optic disc of dice metric and the loss acquired from trained data.
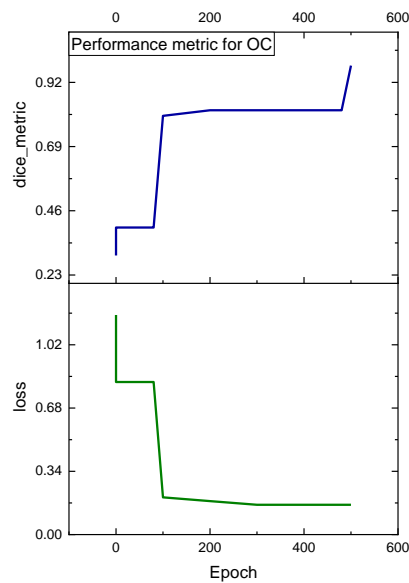

Figure 11 .Data from trained data versus optic cup of dice metric comparison graph

At a learning rate of 0.001, both the OC and OD divisions become more perfect. There was no error in the suggested method using the two convolutional Glaucoma detection neural network designs with down and up sampling layers. Neural network design. To train the NVIDIA design in the given model, the U-net design with regular layout needs 10 hours .

Table 2 .The result of the proposed model with various learning rate.

Approach	Epoch	Dice Metric (Disc)	Dice Metric (Cup)
Existing Method 1	1000	0.84	0.83
Existing Method 2	1000	0.89	0.87
Existing Method 3	1000	0.94	0.95

Existing Method 4	500	0.96	0.92
Existing Method 5	500	0.94	0.94
Existing Method 6	500	0.94	0.95
Improved DCNN with TL Proposed Method	500	0.9634	0.9614

9. CONCLUSION

Glaucoma severity is directly connected to the expansion of the optic disc cup, even when the two traits are unrelated. The CDR and ISNT readings were found to be efficient in diagnosing glaucoma when machine learning techniques were used. To gain a better understanding of the human eye, we developed a mathematical model to aid in identifying the optic disc and optic cup borders in retinal fundus pictures. This information will aid in the analysis, classification, and grading of glaucoma by assisting with the Cup-to-Disc ratio (CDR), Neuro Retinal Rim Area, and other critical glaucoma analysis, classification, and disease grading criteria. We were able to improve on the present segmentation outcomes by using the model. The proposed method made use of deep neural networks to precisely locate the optic disc and optic cup borders of the eye. Improved DCNN with Transfer Learning can be used to solve this problem. For instance, many degrees of information can be collected from an input image to distinguish between glaucomatous and non-glaucomatous images. The conventional way of division was based on the use of super pixels, shapes, and graph cut models, all of which rely on hand-crafted details and a thorough understanding of the customer's needs to achieve accurate results. Methods focused on low-level criteria like local quality often miss out on subtle visual differences. Similarly, the methodological procedure relies on accurately converting a greater number of parameters, which restricts the applicability of the method. To determine the CDR value, the authors of this study used an effective glaucoma structure that causes the optic disc and cup to become fragmented. A Improved Deep Convolutional Neural Network with Transfer learning was used in conjunction with a deep learning technique to treat glaucoma. This method is 96 percent accuracy proved the   outperformance compared with the other methods.

REFERENCES

1. World Health Organization. Bulletin of the World Health Organization, Vol 82(11). 2004. http://www.who.int/bulletin/volumes/82/11/en/infocus.pdf?ua=1. Accessed 5 May 2016.
2. Bourne RRA. Worldwide glaucoma through the looking glass. Br J Ophthalmol. 2006;90:253–4. https://doi.org/10.1136/bjo.2005.083527.
3. Bock R, Meier J, Nyúl LG, Hornegger J, Michelson G. Glaucoma risk index: automated glaucoma detection from color fundus images. Med Image Anal. 2010;14:471–81. https://doi.org/10.1016/j.media.2009.12.006.
4. Sivaswamy J, Krishnadas SR, Joshi GD, Jain M, Ujjwal A, ST Drishti. Retinal image dataset for optic nerve head (ONH) segmentation. In: 2014 IEEE 11th international symposium on biomedical imaging (ISBI). 2014, p. 53–6. https://doi.org/10.1109/ISBI.2014.6867807.
5. Morales S, Naranjo V, Angulo J, Alcañiz M. Automatic detection of optic disc based on PCA and mathematical morphology. IEEE Trans Med Imag. 2013;32:786–96. https://doi.org/10.1109/TMI.2013.2238244.
6. H.N.Veena ,et al.”A Novel Optic disc and optic cup segmentation technique to diagnose glaucoma using deep learning convolutional neural network over retinal fundus images “,Journal of King saud university Computer and Information Science
7. Fu, Huazhu, et al. "Joint optic disc and cup segmentation based on multi-label deep network and polar transformation." arXiv:1801.00926, 2018.
8. M. Sarathi, M. Dutta, A. Singh and C. Travieso, "Blood vessel inpainting based technique for efficient localization and segmentation of optic disc in digital fundus images", Biomedical Signal Processing and Control, vol. 25, pp. 108-117, 2016. doi: 10.1016/j.bspc.2015.10.012
9. Ajeesha and A. Kumar, " Efficient Optic Disc Segmentation and Peripappilary Atropy Detection in Digital Fundus Images", International Journal for Innovative Research in Science & Technology, vol 3, pp. 213-222, 2016.
10. S. Pal and S. Chatterjee, "Mathematical morphology aided optic disk segmentation from retinal images," 2017 3rd International Conference on Condition Assessment Techniques in Electrical Systems (CATCON), Rupnagar, pp. 380-385, 2017, doi: 10.1109/CATCON.2017.8280249.
11. A. Septiarini, A. Harjoko, R. Pulungan, R. Ekantini, "Optic disc and cup segmentation by automatic thresholding with morphological operation for glaucoma evaluation", Signal Image Video Process., vol. 11, no. 5, pp. 945-952, 2017
12. A. Almazroa, W. Sun, S. Alodhayb, K. Raahemifar and V. Lakshminarayanan,"Optic disc segmentation for glaucoma screening system using fundus images", Clinical Ophthalmology, vol. 11, pp. 2017-2029, 2017. doi: 10.2147/opth.s140061.
13. J. Ayub, J. Ahmad, J. Muhammad, L. Aziz, S. Ayub, U. Akram, andI. Basit. Glaucoma detection through optic disc and cup segmentationusing K-mean clustering. In 2016 International Conference onComputing, Electronic and Electrical Engineering (ICE Cube), pages

14. S.M. Nikam and C.Y. Patil. Glaucoma detection from fundus imagesusing matlab gui. In 2017 3rd International Conference on Advancesin Computing, Communication & Automation (ICACCA)(Fall), pages1–4, 2017.

15. Chrástek, R., Wolf, M., Donath, K., Michelson, G., Niemann, H., 2002. Optic disc segmentation in retinal images. Bildverarbeitung für die Medizin 2002, 263– 266.

16. Chen, X., Xu, Y., Yan, S., Wong, D.W.K., Wong, T.Y., Liu, J., 2015. Automatic feature learning for glaucoma detection based on deep learning. In: International Conference on Medical Image Computing and Computer-Assisted Intervention, pp. 669–677.

17. Jiang, Yuming et al., 2019. Jointrcnn: a region-based convolutional neural network for optic disc and cup segmentation. IEEE Trans. Biomed. Eng. 67 (2), 335–343.

18. M.Juneja, S. Singh, N. Agarwal, S. Bali, S. Gupta, N. Thakur and P. Jindal, ''Automated detection of Glaucoma using deep learning convolution network (G-net)'',

19. Multimedia Tools and Applications,pp.1-23,2019.

20. Raghavendra, U., Fujita, H., Bhandary, S.V., Gudigar, A., Tan, J.H., Acharya, U.R., 2018. Deep convolution neural network for accurate diagnosis of glaucoma using digital fundus images. Inf. Sci. 441, 41–49.

21. Zilly, J.G., Buhmann, J.M., Mahapatra, D., 2015. Boosting convolutional filters with entropy sampling for optic cup and disc image segmentation from fundus images. International workshop on machine learning in medical imaging, Springer, Cham.

22. Zilly, J., Buhmann, J.M., Mahapatra, D., 2018. Glaucoma detection using entropy sampling and ensemble learning for automatic optic cup and disc segmentation. Comput. Med. Imaging Graph. 55, 28–41.

23. Mathews, Priya M., et al. "Etiology of global corneal blindness and current practices of corneal transplantation: a focused review." Cornea 37.9 (2018):1198-1203.

24. Wong, Kah Hie, et al. "Corneal blindness and current major treatment concern-graft scarcity." International journal of ophthalmology 10.7 (2017):1154.

25. Almazroa, Ahmed, et al. "Retinal fundus images for glaucoma analysis: the RIGA dataset." Medical Imaging 2018: Imaging Informatics for Healthcare, Research, and Applications. Vol. 10579. International Society for Optics and Photonics,2018.

26. Sengupta, Sourya, et al. "Application of Deep Learning in Fundus Image Processing for Ophthalmic Diagnosis--A Review." arXiv preprint arXiv:1812.07101 (2018).

27. Singh, Amitojdeep, Sourya Sengupta, and Vasudevan Lakshminarayanan. "Glaucoma diagnosis using transfer learning methods." Applications of Machine Learning. Vol. 11139. International Society for Optics and Photonics,2019.

28. Krishna, Komanduri Venkata Sesha Sai Rama, et al. "Classification of Glaucoma Optical Coherence Tomography (OCT) Images Based on Blood Vessel Identification Using CNN and Firefly Optimization." Traitement du Signal 38.1 (2021):239-245.

29. Acharya, U. Rajendra, et al. "Decision support system for the glaucoma using Gabor transformation." Biomedical Signal Processing and Control 15 (2015):18-26.

30. Raghavendra, U., et al. "Deep convolution neural network for accurate diagnosis of glaucoma using digital fundus images." Information Sciences 441 (2018):41-49.

31. Fu, Huazhu, et al. "Disc-aware ensemble network for glaucoma screening from fundus image." IEEE transactions on medical imaging 37.11 (2018):2493-2501.

32. Acharya, U. Rajendra, et al. "A novel algorithm to detect glaucoma risk using texton and local configuration pattern features extracted from fundus images." Computers in biology and medicine 88 (2017):72-83.

33. Yin, Pengshuai, et al. "PM-Net: Pyramid multi-label network for joint optic disc and cup segmentation." International Conference on Medical Image Computing and Computer-Assisted Intervention. Springer, Cham,2019.

34. Fu, Huazhu, et al. "Joint optic disc and cup segmentation based on multi-label deep network and polar transformation." IEEE transactions on medical imaging 37.7 (2018):1597-1605.

35. Jiang, Yuming, et al. "JointRCNN: a region-based convolutional neural network for optic disc and cup segmentation." IEEE Transactions on Biomedical Engineering 67.2 (2019):335-343.

36. Chakravarty, Arunava, and Jayanthi Sivaswamy. "Joint optic disc and cup boundary extraction from monocular fundus images." Computer methods and programs in biomedicine 147 (2017):51-61.

37. Dashtbozorg,Behdad,AnaMariaMendonça,andAurélioCampilho."Opticdiscsegmentationusingthe sliding band filter." Computers in biology and medicine 56 (2015):1-12.

38. Araújo, José Denes Lima, et al. "Glaucoma diagnosis in fundus eye images using diversity indexes." Multimedia Tools and Applications 78.10 (2019): 12987-13004.

39. Li, Annan, et al. "Learning supervised descent directions for optic disc segmentation." Neurocomputing 275 (2018):350-357.

40. Sharma, Ambika, et al. "Automatic glaucoma diagnosis in digital fundus images using deep CNNs." Advances in Computational Intelligence Techniques. Springer, Singapore, 2020.37-52.

41. Ronneberger, Olaf, Philipp Fischer, and Thomas Brox. "U-net: Convolutional networks for biomedical image segmentation." International Conference on Medical image computing and computer-assisted intervention. Springer, Cham,2015.

42. Sevastopolsky, Artem. "Optic disc and cup segmentation methods for glaucoma detection with modification of U-Net convolutional neural network." Pattern Recognition and Image Analysis 27.3 (2017):618-624.

43. Sevastopolsky, Artem, et al. "Stack-u-net: Refinement network for image segmentation on the example of optic disc and cup." arXiv preprint arXiv:1804.11294(2018).

44. Sandler, Mark, et al. "Mobilenetv2: Inverted residuals and linear bottlenecks." Proceedings of the IEEE conference on computer vision and pattern recognition.2018.